# Short, Cold, and Mostly Dry Conditions in Nili Planum Leading to the Olivine-Carbonate Unit Formation: Results from Reactive Transport Modeling

Sierra Vivian Kaufman[1], John F Mustard[1], Kate Maher[2], and Peter B Kelemen[3]

[1]Brown University
[2]Stanford University
[3]Columbia University

November 22, 2022

## Abstract

In Nili Planum, the olivine-bearing unit covering large portions of this region is variably altered to produce the most expansive carbonate detection on Mars. The mechanism of carbonation is unknown. Here we test the conditions necessary to form the olivine-carbonate unit using the reactive transport model (RTM), CruchFlow. The continued presence of olivine requires a short duration of alteration, and/or limited fluid-rock ratios. Furthermore, temperatures must have been low to form a layer of the olivine-carbonate unit consistent with the observed thicknesses. Water availability must have been insufficient to prevent significant amounts of unobserved phases from forming, (e.g., talc, serpentine, and brucite) which would be consistent with alteration pathways on Earth that form carbonate from olivine. The Perseverance rover can make measurements of this unit, providing the data necessary to constrain its formation conditions further.

## Hosted file

essoar.10510530.1.docx available at https://authorea.com/users/535378/articles/598741-short-cold-and-mostly-dry-conditions-in-nili-planum-leading-to-the-olivine-carbonate-unit-formation-results-from-reactive-transport-modeling

1

**Short, Cold, and Mostly Dry Conditions in Nili Planum Leading to the Olivine-Carbonate Unit Formation: Results from Reactive Transport Modeling**

**S. V. Kaufman[1], J. F. Mustard[1], K. Maher[2] and P. B. Kelemen[3]**

[1]Department of Earth, Environmental, and Planetary Sciences, Brown University, Providence, RI 02912

[2]Department of Earth System Science, Stanford University, Stanford, CA 94305

[3]Department of Earth & Environmental Sciences, Columbia University, New York City, NY 11027

Corresponding author: Sierra V. Kaufman (sierra_kaufman@brown.edu)

**Key Points:**

- The olivine-carbonate unit in Nili Planum can be reproduced in a top down aqueous alteration scenario through reactive transport modeling.

- The alteration must occur in a water limited environment to prevent phases not observed in ortibal spectra from forming in high quantities.

- Lower temperature alteration favors the production of a thicker unit consistent with previous observations.

**Abstract**

In Nili Planum, the olivine-bearing unit covering large portions of this region is variably altered to produce the most expansive carbonate detection on Mars. The mechanism of carbonation is unknown. Here we test the conditions necessary to form the olivine-carbonate unit using the reactive transport model (RTM), CruchFlow. The continued presence of olivine requires a short duration of alteration, and/or limited fluid-rock ratios. Furthermore, temperatures must have been low to form a layer of the olivine-carbonate unit consistent with the observed thicknesses. Water availability must have been insufficient to prevent significant amounts of unobserved phases from forming, (e.g., talc, serpentine, and brucite) which would be consistent with alteration pathways on Earth that form carbonate from olivine. The Perseverance rover can make measurements of this unit, providing the data necessary to constrain its formation conditions further.

**Plain Language Summary**

In Nili Planum (the area of Mars where Jezero crater-the landing site of the Perseverance rover-is located), there is a unit of rock containing large proportions of olivine which has been irregularly altered to carbonate. Here we explore the hypothesis that the carbonate formed from the reaction of olivine with liquid water and use computer modeling to determine the conditions that would have been present to form this unique unit. We find temperatures must have been low and water must have been present in very low amounts otherwise the layer would be smaller (higher temperature) or contain other minerals we don't see (more water). These results help us understand the conditions that were present on early Mars. The measurements from Perseverance will help provide further data necessary to understand the origin of this unit further.

**1 Introduction**

The olivine-carbonate unit in Nili Planum is the most extensive carbonate exposure on Mars (Ehlmann et al., 2008). This unit is composed of olivine-enriched rocks of basaltic composition (Edwards & Ehlmann, 2015; Salvatore et al., 2018), variably altered to carbonate (Edwards & Ehlmann, 2015; Tarnas et al., 2021), and has a friable, clastic texture (Rogers et al., 2018) (possibly consistent with an airfall pyroclastic deposit (Kremer et al., 2019)). The hypotheses for carbonate formation in Nili Planum include: *(1)* alteration of the olivine through surface weathering (Brown et al., 2020; Doran et al., 1998; Kelemen et al., 2020), *(2)* hydrothermal/subsurface alteration (van Berk & Fu, 2011; Brown et al., 2010; Edwards & Ehlmann, 2015; Viviano et al., 2013), and *(3)* direct precipitation (Horgan et al., 2020; Ruff et al., 2014). The detection of carbonate indicates that conditions, including the presence of liquid water, were conducive to its formation at some point during or after the emplacement of the unit in the Noachian (Ehlmann et al., 2008).

During the Late Noachian/Early Hesperian period, there is abundant evidence for warm and wet conditions, including fluvial features on the surface (e.g., Carr, 1996; Irwin et al., 2008) as well as alteration minerals such as smectite clays, hydrated silica and carbonate (Bibring et al., 2006; Edwards & Ehlmann, 2015; Murchie et al., 2009). However, robust 3D climate models do not support the presence of liquid water on the surface for extended periods (i.e., Forget et al., 2013; Wordsworth et al., 2013, 2015). This is due to the faint young sun (Sagan & Mullen, 1972) that would have fostered a cold and icy background climate throughout much of Early Mars' history (Head & Marchant, 2014). Previous researchers have shown punctuated heating events, such as

62  impacts (Palumbo & Head, 2018; Segura et al., 2002, 2008; Toon et al., 2010), volcanism
63  (Halevy & Head III, 2014), and changes in eccentricity and obliquity (Palumbo et al., 2018), can
64  give rise to the temperatures necessary to form fluvial features. However, it is unknown if such
65  punctuated events can produce liquid water in contact with rock long enough to create hydrous
66  mineralogy.

67  To test the hypotheses that olivine carbonation occurred (via reaction of aqueous fluid with
68  rocks) in a near-surface environment on Mars during the Late Noachian/Early Hesperian, we use
69  a reactive transport model (RTM) to simulate gravity-driven flow of water through a mafic
70  porous medium enriched in olivine (as established by remote sensing and now Perseverance
71  Rover observations) (Mandon et al., 2021). We vary ambient climatic/atmospheric conditions
72  and protolith composition and assess the resulting mineralogy. Results are compared to previous
73  work that constrained the unit's composition and mineralogy through remote sensing (Brown et
74  al., 2020; Salvatore et al., 2018). Our results can further be compared to measurements from the
75  Perseverance rover, which has been exploring rocks in Jezero Crater since 2/18/2021.

## 2 Materials and Methods

77  We used the RTM CrunchFlow (Steefel et al., 2015), a Global Implicit Multicomponent Reactive
78  Transport (GIMRT) solver, that accccounts for advection, diffusion/dispersion and chemical
79  reactions, both equilibrium and kinetic (Steefel & Lasaga, 1994; Steefel & MacQuarrie, 1996).

80  Initial conditions for each simulation are a one-dimensional 25 m column with 5 cm
81  discretization and 40% porosity to allow for fluid flow and account for the unit's observed
82  friable, clastic nature (Rogers et al., 2018). Porosity, surface area, and mineral volumes evolve
83  for 100,000 years, with output a every half order of magnitude and 10,000 years or until they
84  encounter a physically justified error such as pore closure. Permeability was linked to porosity
85  evolution using the Kozeny-Carman relationship such that if porosity decreases, fluid flow must
86  decrease. Fluid flows from the top of the column, implying a source from precipitation or
87  another top-down driven delivery mechanism. The resulting initial darcy flux through the
88  column was 1.26 m/yr. Liquid saturation is specified at 100% and 1% such that for simulations
89  with <100% saturation, $CO_2$(gas) is present in the pore space resulting in an open system
90  (Winnick & Maher, 2018). We model the atmosphere as pure $CO_2$ with runs at 0.5, 1, and 2 bar,
91  consistent with estimates for the Noachian period from the MAVEN mission (Kurokawa et al.,
92  2018).

93  The initial fluid is consistent with dilute precipitation and does not affect the outcome. We use
94  the chlorine anion to charge balance the system due to its abundance in Mars soil (Clark et al.,
95  1982). The pH of incoming water is varied in 1 unit increments from 3 to 9, encompassing pH
96  values reported for other areas on Mars, including formation of jarosite and the assemblage at the
97  Phoenix landing site (e.g., Kounaves et al., 2010; McLennan et al., 2005) When testing the pH
98  effets, we hold $P_{CO2}$ constant and vary pH by changing alkalinity.

99  In one set of simulations (referred to as the "restricted set"), we restrict the possible alteration
100  products to carbonate and amorphous silica. This allows the effects of the changing variables to
101  be independently assessed, and additional alteration mineralogy is added later. We vary
102  temperature, pH of incoming water, atmospheric pressure of $CO_2$, and primary mineralogy to
103  determine the effect of each variable on the resulting mineralogy and extent of alteration (Table
104  1). We test each variable independently and keep all others at base model conditions (Table 1).

105    Temperature ranges from 0 ℃ to 40 ℃ with intermediate runs at 10, 15, 25, and 30 ℃. Below 0
106    ℃, the water is in a solid phase, suspending any reaction.

107    Within the restricted set, we tested if adding pyroxene and plagioclase would appreciably change
108    our results and found they did not. Therefore, to simplify the model reactions and runtime, we
109    substituted these minerals with a nonreactive mineral phase (herein referred to as gray mineral).
110    This phase is modeled as 75% by volume of non-pore space mineralogy, consistent with
111    previous work showing 20-25% olivine in these basalts (Edwards & Ehlmann, 2015). Olivine
112    chemistry is varied from $Fo_{40}$ to $Fo_{100}$ in 10% increments consistent with previous estimates
113    (Brown et al., 2020; Edwards & Ehlmann, 2015; Hamilton & Christensen, 2005).

114    We created a few combination scenarios for the primary mineralogy to explore more realistic
115    scenarios closer to orbital and rover measurements. The combination scenarios all held gray
116    mineral constant at 75% by volume of non-pore space mineralogy and varied the remaining
117    mineralogy from 40% forsterite (60% fayalite) to 70% forsterite (30% fayalite).

118    In a second set of simulations (the "unsuppressed set"), we included secondary mineral
119    assemblages typical of mafic and ultramafic rocks altering to carbonate, including brucite,
120    serpentine, and talc. To simplify the kinetics, we focused solely on the magnesium endmembers.

121    Although many minerals have several dissolution (and precipitation) mechanisms, we chose to
122    include a smaller subset of possible kinetic reactions and specify the parameters used in Table 2.
123    We assume that the rate law is reversible through equilibrium for all mineral kinetics listed
124    herein. Primary mineralogy (forsterite and fayalite) has a specific surface area (SSA) of $3.3 \times 10^{-4}$
125    $m^2/g$, and all secondary mineralogy has an initial SSA of 30 $m^2/g$. We obtained thermodynamic
126    parameters from the database utilized by CrunchFlow, EQ3/6 (Wolery et al., 1990).
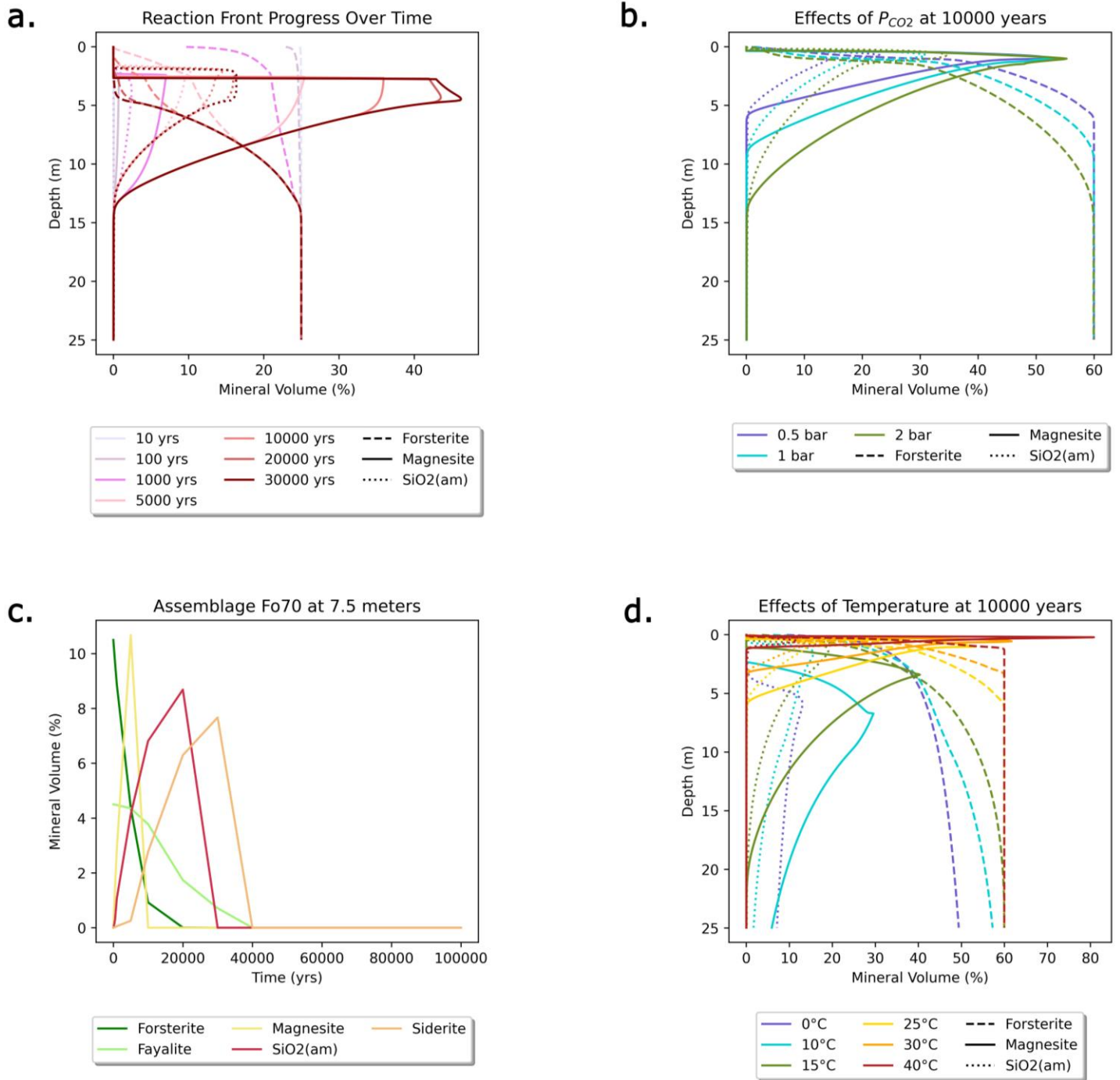
**Figure 1**. *Results from selected mineralogy-restricted model runs. a) The progression of the reaction front over time; as time moves forward more olivine is dissolved and more magnesite/amorphous silica is produced. Note the area that forms at the top of the column with no olivine or alteration mineralogyb) The effects of $P_{CO2}$ after 10,000 years. Increased $P_{CO2}$ increases reaction rates and pushes the reaction front down the column faster. c) The alteration assemblage produced by reaction with 70% forsterite and 30% fayalite. Plots a and c included a*

133     *nonreactive gray mineral phase compromising 35% of the volume, and all runs started with 40%*
134     *porosity. d) The effects of temperature after 10,000 years.*

135     **3 Results**

136     The tested variables had differing effects on the outcome of the model runs (Figure 1). The
137     variation of the initial pH had the most negligible impact, with  differences arising at the very top
138     of the column early in the run. As the reactions progress, the pH is set by mineral dissolution and
139     precipitation, approaching neutral throughout the column.

140     Atmospheric $CO_2$ levels have more impact on the resulting mineralogy. The change from 0.5 to
141     2 bars $CO_2$ causes the volume of solid products to increase by ~10%, the volume of solid
142     reactants to decrease by approximately the same amount, because higher $CO_2$ levels produce
143     faster olivine dissolution  and carbonate precipitation.

144     The most sensitive variable is temperature (Figure 1d). Higher temperatures drive both faster
145     dissolution of olivine and precipitation of carbonate. However, as temperataures approach 40˚C,
146     the rapid carbonate precipitation results in pore closure and near cesssation of flow which
147     effectively shut down the reactions after just 500 years, preventing further carbonate formation
148     and restricting the depth interval of alteration to 1.25 m. In contrast, at 0 °C, olivine dissolves
149     slowly and no carbonate forms.

150     Based on previous work (Brown et al., 2020; Salvatore et al., 2018), we ran models for a range
151     of possible olivine forsterite contents (Mg#) (Table 1). We did not directly vary the forsterite
152     content of the olivine. Instead, we used varying proportions of forsterite and fayalite (Figure 1c),
153     relying on previously established rate laws (Table 2) for each mineral rather than calculating
154     rates based on assumptions of the type of mixing in olivine solid solutions. Under an acid
155     mechanism, fayalite dissolves faster than forsterite by an order of magnitude (thereby producing
156     more dissolved $Fe^{2+}$ and promoting siderite precipitation over magnesite); the reverse is true
157     during neutral dissolution. In our models, the solution is buffered to circum neutral regardless of
158     the pH of the incoming water, causing the neutral olivine dissolution mechanism to dominate.

159     All runs described above restricted the possible secondary mineralogy to carbonate phases and
160     amorphous silica. Typical reaction pathways for olivine carbonation move through a mixed
161     phase of serpentine, brucite, and talc. By allowing these hydrous minerals to precipitate in a
162     pore-filled fluid flow environment, these phases dominated the resulting facies, resulting in over
163     more than 40% talc and serpentine by volume. However, restricting water saturation to 1% of the
164     pore space caused only a small amount of talc to precipitate, and this, decreased with time
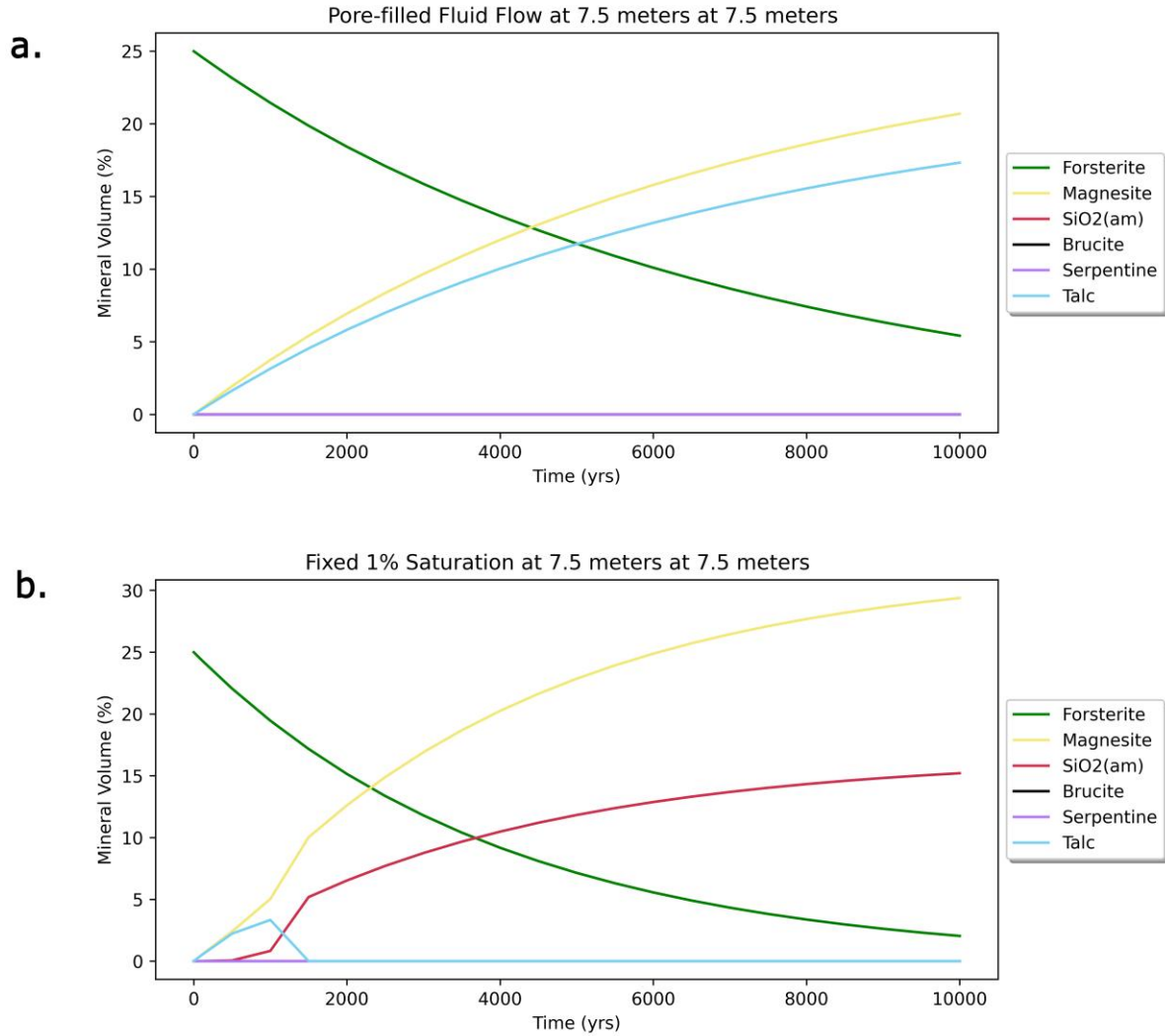165     (Figure 2).

a.

Pore-filled Fluid Flow at 7.5 meters at 7.5 meters

b.

Fixed 1% Saturation at 7.5 meters at 7.5 meters

166

**Figure 2**. *Results from selected unsupressed runs: a) The alteration assemblage produced by reaction of forsterite-bearing rock with fluid flowing through water-filled pores (later timesteps reach >40% of phases that are rare or absent in spectral studies of the olivine-carbonate unit). b) This same run as (a) with only 1% of the pore space filled with water.*

## 4 Discussion

These models explore an alteration regime in which water enters the column from above, creating mineral dissolution and precipitation reaction fronts that migrate over time. Olivine preferentially dissolves due to its lower stability, and carbonate and silica precipitate in the pore space, pressumably as rinds on the grains or pore-filling precipitates. In CRISM data (Figure 3a), the cohesive exposures of the olivine-carbonate unit (Figure 3b) commonly show spectral features of both olivine and carbonate (Figure 3d). Nearby dunes (Figure 3c) show strong olivine spectral signatures but no evidence of carbonate minerals (Figure 3e). We suggest that during physical weathering and disaggregation of the carbonate-bearing bedrock, carbonate is preferentially broken into fine grains and removed by eolian processes, while olivine crystals are preferentially retained locally in dunes. For example, if the carbonate is precipitated as rinds,

182  saltation of olivine-carbonate grains would cause the much softer carbonate to abrade away,
183  leaving only the olivine (Figure 3g). The abraded carbonate may contribute to carbonate detected
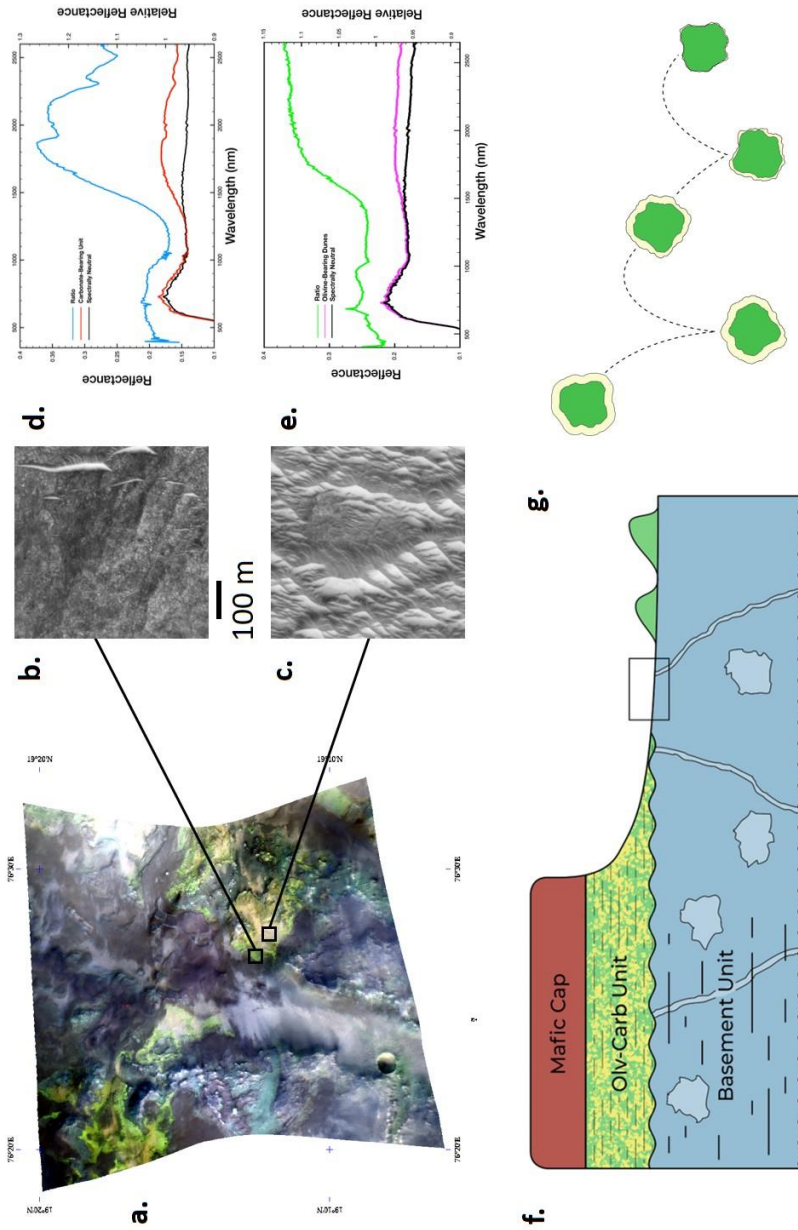184  in the martian dust (Bandfield et al., 2003).



185

186  **Figure 3**. *a. CRISM observation 000093be with surface reflectance in R=2.3, G=1.8, and*
187  *B=1.08 μm, (Seelos, 2016) b/c. Full resolution close-up extracted from HiRISE image*
188  *PSP_006778_1995 (McEwen, 2017). Note the impressive dunes observed in HiRISE from the*
189  *olivine-rich region (c) compared to the smooth outcrops from the magnesite-rich region (b) d.*
190  *CRISM spectra of carbonate-bearing (red) and spectrally neutral regions (black) and their ratio*
191  *(blue). The ratio spectrum shows diagnostic absorptions due to magnesite near 2300 and 2500*
192  *nm. e. CRISM spectra of olivine-bearing (magenta) and spectrally neutral regions (black) and*
193  *their ratio (green). The ratio spectrum shows diagnostic absorptions due to Fe$^{2+}$ in olivine near*

*1000 nm. **f.** A simplified stratigraphic column for this area (Bramble et al., 2017; Ehlmann & Mustard, 2012; Scheller & Ehlmann, 2020). The mafic capping unit is shown on the top in maroon/red color; the olivine-carbonate unit is below this in a green and yellow speckled color with banding shown in the unit; below this is the Noachian basement unit shown in blue with ridges (Pascuzzo et al., 2019), megabreccia, and layering in the western portion. Olivine dunes are depicted on top of the basement unit. **g.** Blow-up of the black box in panel F. The olivine grains physically erode the magnesite layer through saltation, causing only the olivine to remain in the dunes.*

The olivine-carbonate unit in Nili Planum has an average thickness of ~10 m, with some partial sections in Libya Montes measuring up to ~104 m (Kremer et al., 2019). We find that carbonate/silica precipitation causes pore closure in high-temperature runs, preventing further alteration. The layer thickness produced by higher temperature runs, with high water availability, is small and therefore is inconsistent with the observed thickness of the unit. Low temperatures (>0 °C) are more conducive to forming thicker units consistent with the observed mineralogy. However, when incorporating precipitation of hydrous silcate minerals, runs at higher water availability form talc, serpentine and brucite. There have been small amounts of talc found in this region (Brown et al., 2010; Viviano et al., 2013). However, these detections are not widespread or in the modeled quantities (up to ~40%). Previous researchers suggested that low water activity during olivine alteration to carbonate would prevent large quantities of talc, serpentine and brucite (Kelemen et al., 2020). Similarly, simulations wtih minimal amounts of water show a short period in which a small volume percentage of talc forms, but carbonate and amorphous silica continue to dominate the modeled alteration mineralogy shortly after (Figure 2b). Thus, the observed mineralogy in this region is consistent with a top-down alteration mechanism, given low water availability and low temperatures.

The initial volume of olivine controls the amount of carbonate that can form. Our model runs showed plagioclase and pyroxene do not dissolve significantly in relevant timescales (short enough that relict olivine is present) under these conditions. Olivine is substantially less stable and preferentially dissolves, providing the necessary components ($Fe^{2+}$, $Mg^{2+}$) to form the carbonates. The plagioclase and pyroxene were replaced with gray mineral to simplify model calculations. The less olivine present, the less carbonate formed. Once the olivine is completely reacted, the previously precipitated carbonate then becomes undersaturated and dissolves, consistent with the co-occurence of olivine and carbonate in this unit. As the olivine dissolves from the top of the column downward, it ceases to be present in the topmost portion of the column. Without olivine present to provide iron and magnesium ions, the carbonate soon dissolves and moves down the column, following closely behind the olivine, consistent with the co-occurrence of the olivine and carbonate in this unit (Ehlmann et al., 2008). Over long timescales, this can create a portion of the column above the olivine and carbonate that still contains the less reactive primary mineralogy but does not have carbonate.This domain may represent the equivalent of the mafic capping unit stratigraphically above the olivine-carbonate unit (Figure 3f); the capping unit and olivine-carbonate unit share many of the same physical characteristics, extent, and formation hypotheses (Hundal et al., 2020). Further modeling focused on formation of the capping unit, together with geomorphic observations, could investigate whether the two layers share an emplacement and alteration origin.

Previous observations have shown the carbonate contains both iron and magnesium (siderite and magnesite), where magnesite predominates (Brown et al., 2010; Edwards & Ehlmann, 2015;

239   Tarnas et al., 2021). Due to the pH buffering caused by dissolution, the neutral mechanism for
240   olivine dissolution dominates in all of our models, causing increased forsterite dissolution rates
241   over fayalite dissolution. The dominance of this mechanism causes us to predict magnesite to be
242   more abundant than siderite. (In addition, high supersatution is required for siderite precipitation
243   (Tosca & Jiang, 2020), but kinetic limitations on mineral precipitation are not incorporated in our
244   modeling). Early results from the Perseverance rover show olivine in the region has a Fo# of 70
245   (Wiens et al., 2021); Figure 1c shows modeling results of using this olivine composition, in
246   which magnesite precipitates quickly, then dissolves when the forsterite is exhausted. Siderite,
247   however, is predicted to precipitate more slowly and persists for longer. Amorphous silica also
248   forms from the dissolution of olivine in our model, signatures of which have been found in the
249   spectra of the olivine-carbonate unit (Tarnas et al., 2019).

250   The models used here do not account for transient water availability, temperature, and other
251   conditions. Therefore, the timescales of these results should be considered as cumulative time
252   under these conditions rather than necessarily subsequent years. Nevertheless, the timescales for
253   this alteration are still relatively short, even in cold and low water activity environments such
254   that the formation of the olivine-carbonate assemblage takes only a few thousand model years.
255   Carbonate minerals in mafic Martian meteorites recovered from the Antarctic ice capmay h ave
256   formed under similar conditions (Jull et al., 1988; Velbel et al., 1991).

## 4 Conclusions

258   This study modeled various conditions of top-down, aqueous alteration scenarios to reproduce
259   the mineralogy of the olivine carbonate unit in Nili Planum. Modeling successfully reproduced
260   mineral assemblages inferred in previous orbital spectroscopy studies(Brown et al., 2010, 2020;
261   Edwards & Ehlmann, 2015; Salvatore et al., 2018; Tarnas et al., 2019, 2021). The alteration
262   mineralogy precipitates in the pore space of the initial rock, forming a rind on the original
263   mineral grains. Saltation of these grains during aeolian erosion removes the rind, pulverizing the
264   carbonate into dust (Bandfield et al., 2003) and the olivine into sand. The simulations that
265   successfully reproduced the approximate thickness of the olivine-carbonate unit incorporated low
266   temperatures and low water availability (as previously suggested by (Kelemen et al., 2020)).
267   There must be low water availability to prevent unobserved phases from forming in substantial
268   amounts. We show that the olivine-carbonate unit formed in a relatively short cumulative period,
269   while longer timespans led to complete dissolution of both olivine and carbonate. The formation
270   of this unit creates a layer with the same higher-stability primary mineralogy and without
271   carbonate above it; we suggest this may be related to the mafic capping unit that regionally
272   overlies the olivine-carbonate unit. The results from the Perseverance rover will provide a higher
273   resolution geochemical dataset for this region to compare to these results to constrain the unit's
274   formation conditions further.

## Acknowledgments

280
281

282 **Open Research**

283 CrunchFlow is a DOE funded software package authored by C.I. Steefel, S. Molins, and J. Druhan

284 as described in (Steefel et al., 2015). Crunchflow executable, input, and database files used to

285 generate the data for this paper are archived in Zenodo DOI:10.5281/zenodo.5879909. Figures were

286 produced using Matplotlib 3.4.3 (Figures 1 and 2) and ENVI 5.0 (Figure 3).

287 **References**

288 Bandfield, J. L., Glotch, T. D., & Christensen, P. R. (2003). Spectroscopic Identification of
289 Carbonate Minerals in the Martian Dust. *Science*, *301*(5636), 1084–1087.
290 https://doi.org/10.1126/science.1088054

291 van Berk, W., & Fu, Y. (2011). Reproducing hydrogeochemical conditions triggering the
292 formation of carbonate and phyllosilicate alteration mineral assemblages on Mars (Nili Fossae
293 region). *Journal of Geophysical Research: Planets*, *116*(E10).
294 https://doi.org/10.1029/2011JE003886

295 Bibring, J.-P., Langevin, Y., Mustard, J. F., Poulet, F., Arvidson, R., Gendrin, A., et al. (2006).
296 Global Mineralogical and Aqueous Mars History Derived from OMEGA/Mars Express Data.
297 *Science*, *312*(5772), 400–404. https://doi.org/10.1126/science.1122659

298 Brown, A. J., Hook, S. J., Baldridge, A. M., Crowley, J. K., Bridges, N. T., Thomson, B. J., et al.
299 (2010). Hydrothermal formation of Clay-Carbonate alteration assemblages in the Nili Fossae
300 region of Mars. *Earth and Planetary Science Letters*, *297*(1–2), 174–182.
301 https://doi.org/10.1016/j.epsl.2010.06.018

302 Brown, A. J., Viviano, C. E., & Goudge, T. A. (2020). Olivine-Carbonate Mineralogy of the
303 Jezero Crater Region. *Journal of Geophysical Research: Planets*, *125*(3), e2019JE006011.
304 https://doi.org/10.1029/2019JE006011

305 Carr, M. H. (1996). *Water on Mars*. New York: Oxford University Press.

306 Clark, B. C., Baird, A. K., Weldon, R. J., Tsusaki, D. M., Schnabel, L., & Candelaria, M. P.
307 (1982). Chemical composition of Martian fines. *Journal of Geophysical Research: Solid Earth*,
308 *87*(B12), 10059–10067. https://doi.org/10.1029/JB087iB12p10059

309 Doran, P. T., Wharton, R. A., Marais, D. J. D., & McKay, C. P. (1998). Antarctic paleolake
310 sediments and the search for extinct life on Mars. *Journal of Geophysical Research: Planets*,
311 *103*(E12), 28481–28493. https://doi.org/10.1029/98JE01713

312 Duckworth, O. W., & Martin, S. T. (2004). Role of molecular oxygen in the dissolution of
313 siderite and rhodochrosite1 1Associate editor: U. Becker. *Geochimica et Cosmochimica Acta*,
314 *68*(3), 607–621. https://doi.org/10.1016/S0016-7037(03)00464-2

315    Edwards, C. S., & Ehlmann, B. L. (2015). Carbon sequestration on Mars. *Geology*, *43*(10), 863–
316    866. https://doi.org/10.1130/G36983.1

317    Ehlmann, B. L., Mustard, J. F., Murchie, S. L., Poulet, F., Bishop, J. L., Brown, A. J., et al.
318    (2008). Orbital Identification of Carbonate-Bearing Rocks on Mars. *Science*, *322*(5909), 1828–
319    1832. https://doi.org/10.1126/science.1164759

320    Forget, F., Wordsworth, R., Millour, E., Madeleine, J.-B., Kerber, L., Leconte, J., et al. (2013).
321    3D modelling of the early martian climate under a denser CO2 atmosphere: Temperatures and
322    CO2 ice clouds. *Icarus*, *222*(1), 81–99. https://doi.org/10.1016/j.icarus.2012.10.019

323    Greenberg, J., & Tomson, M. (1992). Precipitation and dissolution kinetics and equilibria of
324    aqueous ferrous carbonate vs temperature. *Applied Geochemistry*, *7*(2), 185–190.
325    https://doi.org/10.1016/0883-2927(92)90036-3

326    Halevy, I., & Head III, J. W. (2014). Episodic warming of early Mars by punctuated volcanism.
327    *Nature Geoscience*, *7*(12), 865–868. https://doi.org/10.1038/ngeo2293

328    Hamilton, V. E., & Christensen, P. R. (2005). Evidence for extensive, olivine-rich bedrock on
329    Mars. *Geology*, *33*(6), 433–436. https://doi.org/10.1130/G21258.1

330    Head, J. W., & Marchant, D. R. (2014). The climate history of early Mars: insights from the
331    Antarctic McMurdo Dry Valleys hydrologic system. *Antarctic Science*, *26*(06), 774–800.
332    https://doi.org/10.1017/S0954102014000686

333    Horgan, B. H. N., Anderson, R. B., Dromart, G., Amador, E. S., & Rice, M. S. (2020). The
334    mineral diversity of Jezero crater: Evidence for possible lacustrine carbonates on Mars. *Icarus*,
335    *339*, 113526. https://doi.org/10.1016/j.icarus.2019.113526

336    Hundal, C., Mustard, J. F., & Kremer, C. H. (2020). Origin of the Pitted Capping Unit in Nili
337    Fossae, Mars. Presented at the 51st Lunar and Planetary Science Conference. Retrieved from
338    https://www.hou.usra.edu/meetings/lpsc2020/pdf/1629.pdf

339    Irwin, R. P., Howard, A. D., & Craddock, R. A. (2008). Fluvial valley networks on Mars. *River
340    Confluences, Tributaries and the Fluvial Network*, 419–451.

341    Jull, A. J. T., Cheng, S., Gooding, J. L., & Velbel, M. A. (1988). Rapid Growth of Magnesium-
342    Carbonate Weathering Products in a Stony Meteorite from Antarctica. *Science*.
343    https://doi.org/10.1126/science.242.4877.417

344    Kelemen, P. B., Evans, O., Ghiorso, M., Mustard, J., Ehlmann, B. L., & Spiegelman, M. (2020).
345    Carbonate in Olivine-Rich Unit(s) on Mars May Have Formed at Low P(H2O). Presented at the
346    51st Lunar and Planetary Science Conference. Retrieved from
347    https://www.hou.usra.edu/meetings/lpsc2020/pdf/1213.pdf

348    Kounaves, S. P., Hecht, M. H., Kapit, J., Gospodinova, K., DeFlores, L., Quinn, R. C., et al.
349    (2010). Wet Chemistry experiments on the 2007 Phoenix Mars Scout Lander mission: Data
350    analysis and results. *Journal of Geophysical Research: Planets*, *115*(E1).
351    https://doi.org/10.1029/2009JE003424

352 Kremer, C. H., Mustard, J. F., & Bramble, M. S. (2019). A widespread olivine-rich ash deposit
353 on Mars. *Geology*, *47*(7), 677–681. https://doi.org/10.1130/G45563.1

354 Kurokawa, H., Kurosawa, K., & Usui, T. (2018). A lower limit of atmospheric pressure on early
355 Mars inferred from nitrogen and argon isotopic compositions. *Icarus*, *299*, 443–459.

356 Mandon, L., Royer, C., Beck, P., Quantin-Nataf, C., Fouchet, T., Poulet, F., et al. (2021).
357 Spectral diversity of rocks and regolith at Jezero crater, Mars, as seen by the SuperCam VISIR
358 spectrometer onboard Perseverance. Presented at the AGU Fall Meeting 2021, AGU. Retrieved
359 from https://agu.confex.com/agu/fm21/meetingapp.cgi/Paper/858074

360 McLennan, S. M., Bell, J. F., Calvin, W. M., Christensen, P. R., Clark, B. C., de Souza, P. A., et
361 al. (2005). Provenance and diagenesis of the evaporite-bearing Burns formation, Meridiani
362 Planum, Mars. *Earth and Planetary Science Letters*, *240*(1), 95–121.
363 https://doi.org/10.1016/j.epsl.2005.09.041

364 Murchie, S. L., Mustard, J. F., Ehlmann, B. L., Milliken, R. E., Bishop, J. L., McKeown, N. K.,
365 et al. (2009). A synthesis of Martian aqueous mineralogy after 1 Mars year of observations from
366 the Mars Reconnaissance Orbiter. *Journal of Geophysical Research*, *114*.
367 https://doi.org/10.1029/2009JE003342

368 Palandri, J. L., & Kharaka, Y. K. (2004). *A compilation of rate parameters of water-mineral
369 interaction kinetics for application to geochemical modeling* (USGS Numbered Series No. 2004–
370 1068). *A compilation of rate parameters of water-mineral interaction kinetics for application to
371 geochemical modeling* (Vol. 2004–1068). U.S. Geological Survey.
372 https://doi.org/10.3133/ofr20041068

373 Palumbo, A. M., & Head, J. W. (2018). Impact cratering as a cause of climate change, surface
374 alteration, and resurfacing during the early history of Mars. *Meteoritics & Planetary Science*,
375 *53*(4), 687–725. https://doi.org/10.1111/maps.13001

376 Palumbo, A. M., Head, J. W., & Wordsworth, R. (2018). Late Noachian Icy Highlands climate
377 model: Exploring the possibility of transient melting and fluvial/lacustrine activity through peak
378 annual and seasonal temperatures. *Icarus*, *300*, 261–286.
379 https://doi.org/10.1016/j.icarus.2017.09.007

380 Rogers, A. D., Warner, N. H., Golombek, M. P., Head, J. W., & Cowart, J. C. (2018). Areally
381 Extensive Surface Bedrock Exposures on Mars: Many Are Clastic Rocks, Not Lavas.
382 *Geophysical Research Letters*, *45*(4), 1767–1777. https://doi.org/10.1002/2018GL077030

383 Ruff, S. W., Niles, P. B., Alfano, F., & Clarke, A. B. (2014). Evidence for a Noachian-aged
384 ephemeral lake in Gusev crater, Mars. *Geology*, *42*(4), 359–362.
385 https://doi.org/10.1130/G35508.1

386 Sagan, C., & Mullen, G. (1972). Earth and Mars: Evolution of Atmospheres and Surface
387 Temperatures. *Science*, *177*(4043), 52–56. https://doi.org/10.1126/science.177.4043.52

Salvatore, M. R., Goudge, T. A., Bramble, M. S., Edwards, C. S., Bandfield, J. L., Amador, E. S., et al. (2018). Bulk mineralogy of the NE Syrtis and Jezero crater regions of Mars derived through thermal infrared spectral analyses. *Icarus*, *301*, 76–96. https://doi.org/10.1016/j.icarus.2017.09.019

Seelos, F. (2016). Mars Reconnaissance Orbiter Compact Reconnaissance Imaging Spectrometer for Mars Map-projected Targeted Reduced Data Record (Version MRO-M-CRISM-5-RDR-MPTARGETED-V1.0) [NASA Planetary Data System].

Segura, T. L., Toon, O. B., Colaprete, A., & Zahnle, K. (2002). Environmental effects of large impacts on Mars. *Science*, *298*, 1977–1980.

Segura, T. L., Toon, O. B., & Colaprete, A. (2008). Modeling the environmental effects of moderate-sized impacts on Mars. *Journal of Geophysical Research*, *113*(E11). https://doi.org/10.1029/2008JE003147

Steefel, C. I., & Lasaga, A. C. (1994). A coupled model for transport of multiple chemical species and kinetic precipitation/dissolution reactions with application to reactive flow in single phase hydrothermal systems. *American Journal of Science*, *294*(5), 529–592. https://doi.org/10.2475/ajs.294.5.529

Steefel, C. I., & MacQuarrie, K. T. B. (1996). Chapter 2. Approaches to Modeling of Reactive Transport in Porous Media. In *Reactive Transport in Porous Media* (Vol. 34). Berlin, Boston: De Gruyter. https://doi.org/10.1515/9781501509797-005

Steefel, C. I., Appelo, C. A. J., Arora, B., Jacques, D., Kalbacher, T., Kolditz, O., et al. (2015). Reactive transport codes for subsurface environmental simulation. *Computational Geosciences*, *19*(3), 445–478. https://doi.org/10.1007/s10596-014-9443-x

Tarnas, J. D., Mustard, J. F., Lin, H., Goudge, T. A., Amador, E. S., Bramble, M. S., et al. (2019). Orbital Identification of Hydrated Silica in Jezero Crater, Mars. *Geophysical Research Letters*, *46*(22), 12771–12782. https://doi.org/10.1029/2019GL085584

Tarnas, J. D., Stack, K. M., Parente, M., Koeppel, A. H. D., Mustard, J. F., Moore, K. R., et al. (2021). Characteristics, Origins, and Biosignature Preservation Potential of Carbonate-Bearing Rocks Within and Outside of Jezero Crater. *Journal of Geophysical Research: Planets*, *126*(11), e2021JE006898. https://doi.org/10.1029/2021JE006898

Toon, O. B., Segura, T., & Zahnle, K. (2010). The Formation of Martian River Valleys by Impacts. *Annual Review of Earth and Planetary Sciences*, *38*(1), 303–322. https://doi.org/10.1146/annurev-earth-040809-152354

Tosca, N., & Jiang, Z. (2020). Growth kinetics of siderite at 298.15 K and 1 bar. *Geochimica et Cosmochimica Acta*, *274*, 97–117. https://doi.org/10.1016/j.gca.2020.01.047

Velbel, M. A., Long, D. T., & Gooding, J. L. (1991). Terrestrial weathering of Antarctic stone meteorites: Formation of Mg-carbonates on ordinary chondrites. *Geochimica et Cosmochimica Acta*, *55*(1), 67–76. https://doi.org/10.1016/0016-7037(91)90400-Y

425 Viviano, C. E., Moersch, J. E., & McSween, H. Y. (2013). Implications for early hydrothermal
426 environments on Mars through the spectral evidence for carbonation and chloritization reactions
427 in the Nili Fossae region. *Journal of Geophysical Research: Planets*, *118*(9), 1858–1872.
428 https://doi.org/10.1002/jgre.20141

429 Wiens, R., Cousin, A., Ollila, A., Beyssac, O., Maurice, S., Johnson, J., et al. (2021). Chemistry,
430 Mineralogy, and Physical Properties of Rocks and Soils Targeted by SUPERCAM at Jezero
431 Crater. Presented at the GSA Connects 2021 in Portland, Oregon, GSA. Retrieved from
432 https://gsa.confex.com/gsa/2021AM/meetingapp.cgi/Paper/367022

433 Winnick, M. J., & Maher, K. (2018). Relationships between CO2, thermodynamic limits on
434 silicate weathering, and the strength of the silicate weathering feedback. *Earth and Planetary*
435 *Science Letters*, *485*, 111–120. https://doi.org/10.1016/j.epsl.2018.01.005

436 Wolery, T. J., Jackson, K. J., Bourcier, W. L., Bruton, C. J., Viani, B. E., Knauss, K. G., &
437 Delany, J. M. (1990). Current Status of the EQ3/6 Software Package for Geochemical Modeling.
438 In *Chemical Modeling of Aqueous Systems II* (Vol. 416, pp. 104–116). American Chemical
439 Society. https://doi.org/10.1021/bk-1990-0416.ch008

440 Wordsworth, R., Forget, F., Millour, E., Head, J. W., Madeleine, J.-B., & Charnay, B. (2013).
441 Global modelling of the early martian climate under a denser CO2 atmosphere: Water cycle and
442 ice evolution. *Icarus*, *222*(1), 1–19. https://doi.org/10.1016/j.icarus.2012.09.036

443 Wordsworth, R., Kerber, L., Pierrehumbert, R. T., Forget, F., & Head, J. W. (2015). Comparison
444 of "warm and wet" and "cold and icy" scenarios for early Mars in a 3-D climate model: Warm
445 and Wet vs. Cold and Icy Early Mars. *Journal of Geophysical Research: Planets*, *120*(6), 1201–
446 1219. https://doi.org/10.1002/2015JE004787

447 **Table 1.** *The explored range for each RTM model variable of interest. The base model column*
448 *represents the default value of a given condition when testing the effects of varying another.*
449

| Variable | Minimum | Maximum | Base Model |
|---|---|---|---|
| **Olivine Fo#** | 40 | 100 | 100 |
| **$P_{CO_2}$** | 0.5 bar | 2 bar | 0.5 bar |
| **Temperature** | 0 °C | 40 °C | 25 °C |
| **pH** | 3 | 9 | Unspecified (neutral) |
| **Vol. Olivine** | 20% | 100% | 100 |

458
459
460
461
462
463
464
465
466

467 **Table 2.** *Name, formula, and kinetic parameters used for each reaction in the model. Minerals listed*
468 *twice have multiple mechanisms included. The rates are reported as log(k) values at 25 °C. The*
469 *activation column lists activation energies in units of kcal/mole. The mechanism column states which*
470 *mechanism from Palandri and Kharaka (2004) is reported.*
471

| Mineral | Formula | Rate (25 °C) | Activation Energy (kcal/mole) | Mechanism[*] |
|---|---|---|---|---|
| **Magnesite**[*] | $MgCO_3$ | -9.34 | 5.62 | Neutral |
| **Siderite** | $FeCO_3$ | -8.65[§] | 25.88[†] | -- |
| **Amorphous Silica**[*] | $SiO_2$ (am) | -12.77 | 16.42 | Neutral |
| **Forsterite**[*] | $Mg_2SiO_4$ | -10.64 | 18.88 | Neutral |
| **Forsterite**[*] | $Mg_2SiO_4$ | -6.85 | 16.06 | Acid |
| **Fayalite**[*] | $Fe_2SiO_4$ | -12.80 | 22.56 | Neutral |
| **Fayalite**[*] | $Fe_2SiO_4$ | -4.80 | 22.56 | Acid |
| **Brucite**[*] | $Mg(OH)_2$ | -8.24 | 10.04 | Neutral |
| **Brucite**[*] | $Mg(OH)2$ | -4.73 | 14.10 | Acid |
| **Serpentine**[*] | $Mg_3Si_2O_5(OH)_4$ | -12.40 | 13.53 | Neutral |
| **Serpentine**[*] | $Mg_3Si_2O_5(OH)_4$ | -5.70 | 18.04 | Acid |
| **Talc**[*] | $Mg_3Si_4O_{10}(OH)_2$ | -12.00 | 10.04 | Neutral |